Redline Atomic-Oxygen-Airglow Image Restoration for the VIOLET CubeSat Mission

Alex L. Voisine
University of New Brunswick
Fredericton, Canada
alex.voisine@ieee.org

Brent R. Petersen
University of New Brunswick
Fredericton, Canada

ABSTRACT

The Spectral Airglow Structure Imager (SASI) is a mission on CubeSat NB's VIOLET satellite, and it is imaging the 630 nm redline atomic oxygen airglow in the ionosphere at altitudes of 300-400 km. The image acquisition conditions of VIOLET make it susceptible to significant degradation primarily due to rotational blurring. A method of deconvolution by ring extraction and linearization using Richardson-Lucy methods for rotational blurring is presented to minimize the rotational blurring in the system. Interpolation by means of splicing and specific pixel deconvolutions are discussed to increase image quality after deconvolution. Boundary conditions for pre-processing to handle corner degradation due to the nature of rotational blurring are also discussed. Preliminary results show effective deconvolution of rotationally blurred images, currently resulting in SSIM indexes approaching 0.50.

CCS CONCEPTS

• **Computing methodologies → Image processing**.

KEYWORDS

Image Processing, CubeSat, Blind Deconvolution, Image Splicing, Interpolation, Motion Blur, Rotational Motion

ACM Reference Format:
Alex L. Voisine and Brent R. Petersen. 2021. Redline Atomic-Oxygen-Airglow Image Restoration for the VIOLET CubeSat Mission. In *10th International Conference on Telecommunications and Remote Sensing (ICTRS '21), November 15–16, 2021, Virtual Conference, Bulgaria.* ACM, New York, NY, USA, 5 pages. https://doi.org/10.1145/3495535.3495538

1 INTRODUCTION

The Spectral Airglow Structure Imager (SASI) is one of two primary missions aboard CubeSat NB's VIOLET CubeSat imaging the redline atomic-oxygen-airglow layer of the ionosphere at the 630 nm wavelength. Due to numerous heavy constraints of the system and the low light conditions of the imaging target, SASI is required to have significant exposure times of up to 7 seconds. Traditionally, long exposure times are compensated for by using very sophisticated attitude control and pointing instrumentation to ensure the imaging target is always in the field [3]. VIOLET does not have any active attitude control due to its power limitations, using only passive magnetic attitude control (PMAC) with a permanent magnet, and will instead be relying on post-processing of the images for increased accuracy.

Accepted Manuscript
ICTRS '21, November 15–16, 2021, Virtual Conference, Bulgaria

ACM ISBN 978-1-4503-9018-7/21/11.
https://doi.org/10.1145/3495535.3495538

There have been several CubeSat missions that include an imager, however they typically image the Earth, which gives off significantly more light than airglow, causing exposure times to decrease. The closest CubeSat resembling VIOLET is the Swiss Cube, a CubeSat imaging airglow with exposure times below a second. They are able to achieve such small exposure times because they were testing an in house sensor technology and telescope design [9]. Due to the uniqueness of the imaging environment and subject, there is insignificant research in the deconvolution of long exposure CubeSat imagery. Motion blur removal is a heavily studied field, and leveraging work in this field is useful in the application. Research done by others in rotational and translational motion blur is discussed in Section 3.

This paper will investigate the rotational motion blur case of atomic-oxygen-airglow imagery as expected from the VIOLET CubeSat. The deconvolution of which leverages the spatially invariant and linear properties of the rotational motion blur kernels along a circular arc. Pre-processing of boundary conditions will also be considered. Finally, the necessity for interpolation in post-processing due to the nature of the deconvolution will be considered.

The rest of the paper is divided into 5 sections. Section 2 describes the background information of the VIOLET project and the orbital dynamics of the system being considered. Section 3 describes the degradation models used for approximation of rotational and translationally blurred images. Section 4 describes the pre-processing and deconvolution methods. Section 5 describes the interpolation used in the research. Section 6 describes the conclusions of the research to this point and the future direction the researchers plan to take.

2 BACKGROUND

Satellite imagery has been a staple of digital image processing research since the early 1960s and the fast evolving space program during that time is often credited with jump starting the field of digital image processing [4]. A CubeSat is a small satellite measured in terms of 10 cm x 10 cm x 10 cm blocks called Units or U for short. CubeSats allow academic institutions to support and grow their space research areas while minimizing the large buy in cost typically associated with breaking into the space sector.

CubeSat NB was selected as one of the groups to partake in the Canadian CubeSat Project, creating a joint project between the University of New Brunswick, l'Université de Moncton, and the New Brunswick Community College in building New Brunswick's first CubeSat, VIOLET. VIOLET is a 2U (10 cm x 10 cm x 20 cm) research satellite for investigating the ionosphere through the use of its two scientific payloads, the GNSS Receiver for Ionospheric

and Position Studies (GRIPS) and the Spectral Airglow Structure Imager (SASI).

Of relevance to the research is the SASI subsystem, a CMOS image sensor imaging the redline airglow layer of the ionosphere at the 630 nm wavelength to investigate the density and location of atomic-oxygen-airglow. The difficulties of imaging this faint oxygen layer with an inexpensive sensor on board a CubeSat are apparent. The main challenge being the requirement for a significantly longer exposure time due to the use of a narrow band redline filter and an inexpensive sensor paired with the low light conditions of space. The requirement of longer exposure times of approximately 3 to 7 seconds has the potential to introduce significant blurring in the resulting images due to the motion of VIOLET during the exposure. The approximation and estimation of the atomic-oxygen-airglow layer relies heavily on the accuracy of the images returned from SASI. The motion blurring introduced into the images creates the additional challenge of determining the true location of the airglow from the blurry images. The key is to properly remove significant amounts of the motion blur, providing an accurate estimation of location, while simultaneously retaining the information present in the image so as not to skew the density of the airglow in the images.

While larger satellites are able to use attitude control systems with very high levels of sophistication and energy usage, CubeSats are extremely limited in their choices for attitude control. This is primarily because as the size of a satellite decreases, so does the available power from the solar panels and the size of the batteries. VIOLET has decided to exclusively use PMAC by including a strong magnet in the center module that will align with Earth's magnetic field. This type of attitude control makes it more difficult to include active control or damping to reduce the blurring of the images. The rotation of VIOLET in various axes will cause different varieties of blurring in the resulting images. Of these blurs, the two most significant types are the linear motion blur caused by the translational motion of VIOLET, and the rotational blur about the +Z axis, the axis in the 20 cm direction, due to the inability for VIOLET to actively dampen its rotation during an exposure period.

3 DEGRADATION MODELS

According to Gonzalez and Woods [4], given that h is a linear, position-invariant process, then the degraded image is given in the spatial domain by

$$Y = h * X + N \tag{1}$$

where Y is the observed image matrix, h is the point spread function (PSF) of the system, $*$ is the two-dimensional convolution operator, X is the true image matrix, and N is the noise matrix present in the system. The goal of a standard deconvolution is to recover X using a combination of the observed image and the PSF, while approximating the noise. This process is known as non-blind deconvolution. The images to be taken by VIOLET will not have an associated PSF with them, and estimating the PSF to recover the true image is a process known as blind deconvolution.

Blind deconvolution is generally an ill-posed problem given the multiple unknown parameters, and accurate image priors should be leveraged if the option exists. For the case of VIOLET, the information about the attitude of the satellite during an exposure is being used to assist in the deconvolution of the images. Of the various types of blur affecting images from VIOLET, the two most significant are the translational and rotational blur about the center +Z axis.

3.1 Translational Blurring

Translational blur has been a heavily studied area of image processing since the early 1960s and is generally not difficult to reverse if the length of the blur can be properly estimated [11]. This is because translational motion blur is spatially invariant and linear, meaning that typical deconvolution methods will work given a proper estimation of the blur kernel. Because of this, research on translational blurring has moved largely towards estimation of the blur lengths [14] [2]. A technique that is heavily leveraged for this task is the Radon Transform, noting its reliability in detecting parallel lines in a Fourier Transform arising from translational motion blur [12]. A linear motion blur can be simulated by a sum of slightly translated images as seen in the top image in Figure 1.

3.2 Rotational Blurring

Rotational blur is significantly more difficult to deal with since it is a non-linear spatially variant blur. This is because the length of the blur is dependant on the distance from the blurring center, in most cases this will be the center of the image. Instances of rotational blurring do not appear as frequently as translational blurring, as such, there is significantly less research in the field. Even less so is the case of a rotating imaging device, as usually rotational blurring research is more in the segmentation of objects rotating in an imaging field [10]. Several research groups opt to use hardware solutions to avoid rotational blurring such as opto-mechanical derotators [1, 13]. Recently, Qiu et al. have applied machine learning to rotational image blur using Conditional Generative Adversarial Networks (CGAN) with good results while also noting that there were no publicly available rotational blurring image repositories and made theirs available [6]. Rotational blurring can be approximated similarly to translational blur except with slight rotations instead of slight translations as seen in the bottom image in Figure 1.

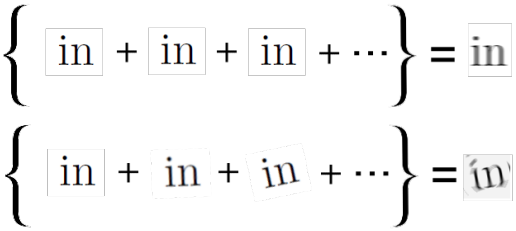

Figure 1: Motion blur approximations: top image is translational blur, bottom image is rotational blur

4 METHODS

The image used for testing and verification is an image of the redline oxygen-airglow layer taken by the Imager of Sprites and Upper Atmospheric Lightnings instrument on-board FORMOSAT-2 operated by the National Space Organization of Taiwan [7]. This

image is a close approximation of what SASI can be expected to take, minus the blurring. The image can be seen in Figure 2

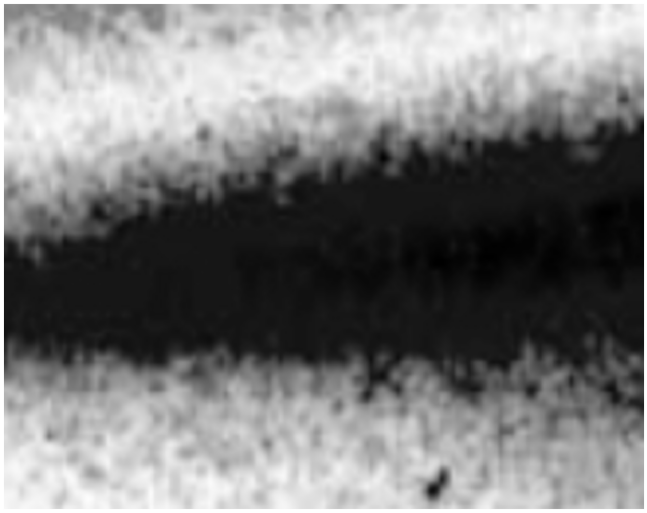

Figure 2: Image used for testing and verification, redline oxygen-airglow image taken by FORMOSAT-2 [7], used with permission from the Wiley Library

4.1 Boundary Conditions

As VIOLET rotates through an exposure period, the corners of the scene are gradually rotated out and the light from those corners is only incident on the sensor for a portion of the exposure. This lack of information causes heavy degradation of the corners of the image in the recovery in the form of ringing artifacts unless proper pre-processing is done. As the rotation angle increases, the amount of data loss in the images also increases. An example of data loss from rotational motion with zero padding as a boundary condition can be seen in Figure 3. In this example, the image is padded with zeros and then rotationally blurred by 10°, then it is padded a second time and then recovered. The degradation of the corners is a direct result of the zero padding, an accurate estimate of outside the scene is necessary for a proper recovery.

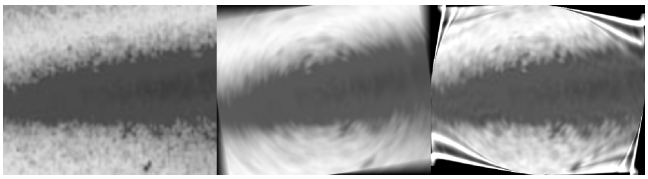

Figure 3: An example of the effects of poor boundary conditions

The image and methods are the same as those in Figure 4, only the boundary condition is changed. The severe ringing artifacts are not seen in Figure 4 due to the nature of pre-processing of boundary conditions of the image. In the case of Figure 4, the input image was padded with reflections of the image during the blurring process and recovery process in order to accurately simulate the blurring conditions and recovery conditions that would be available during a standard image from VIOLET. There are several methods to properly account for this boundary condition and the four that are classically used and have been investigated with this algorithm are padding the image appropriately with either zeros, replicating of the border pixels infinitely, periodically replicating of the image, and reflecting of the image on all sides. Hansen et al. found that replication worked best for the rotational deblurring problem [5].

4.2 Deconvolution

Rotational motion blur can be considered as radially linear, that is to say the rate of change of the length of the blur along a radial path is linear and representable by an arc related to the angular velocity about the +Z axis of the satellite and the exposure time of the image. The relationship between the blurring angle, exposure time and rotational velocity can be seen in Equation 2 and the arc length in Equation 3

$$\theta = T\omega \tag{2}$$

$$s = \frac{2\pi r\theta}{360^\circ} \tag{3}$$

where θ is the blurring angle in degrees, T is the exposure time in seconds, ω is the rotational velocity in the +Z-axis of VIOLET in degrees per second, r is the radius from the center of the image, and s is the arc length in pixels.

The arc length will be equal to the length of the blur in pixels on any given ring radially outward from the center of the image. Each ring can then be treated as a linear motion blur around the ring itself of blur length equal to the arc length. The image can be broken down into individual rings which can then be placed into a vector and treated as a spatially-invariant linear motion blur and solved using conventional deconvolution methods. The rings are pulled out of the image starting at the smallest radius for blurring that corresponds to an arc length of greater than one. The rings are approximated by starting at the input radius and travelling counterclockwise around the image selecting pixels that minimize the difference between the input radius and the pixel radius. The pixels for one ring are then linearized into a vector and a unique linear blur kernel is created with blur length equal to the arc length. The vector is deconvolved using Richardson-Lucy deconvolution [8]. The resulting vector is then remapped to a new image for reconstruction and the algorithm restarts on the next ring. An example of a image that was blurred with 10 degrees rotational blur and reconstructed using this method can be seen in Figure 4.

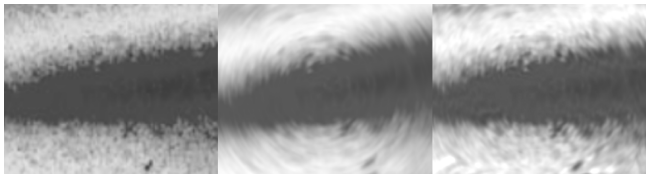

Figure 4: From left to right: Original image, image degraded with 10 degrees rotational motion blur, recovered image.

Closer inspection of a more detailed area of the airglow can be seen in Figure 5. This shows that the deblurring algorithm appears

to correctly restore the shape of specific edges in the image as well as the general intensity of the image, both of which are important to the application.

Figure 5: Zoomed subsection of Figure 4

5 INTERPOLATION

The main drawback that arises in this algorithm is the interpolation of missed points. The need for interpolation is a direct result of the ring algorithm skipping certain pixels between rings, thus never deblurring them. Due to the nature of the ring extraction, cones of lost pixels propagate radially from the center of the images, as seen in Figure 6.

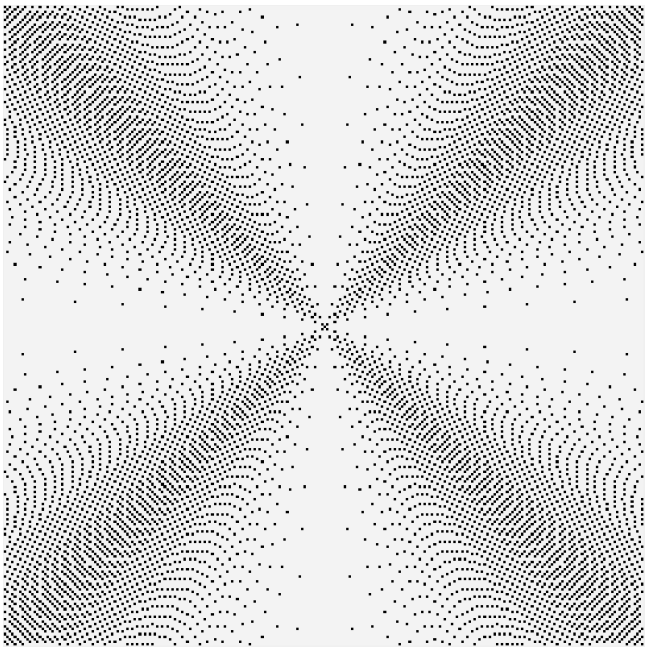

Figure 6: Radial interpolation cones

Specific pixel deconvolution is a method of interpolation that involves identifying specific pixels that require interpolation and determining their specific radius from the center of the image. This radius is then used to extract a corresponding ring from the blurred image which includes the specific pixel. The ring is then deconvolved as normal and inserted into the recovered image, ensuring the pixel that required interpolation is included. This method of interpolation was used in the recovery of Figure 4.

5.1 Image Splicing

Splicing images to minimize interpolation has been researched to greatly reduce the number of pixels requiring interpolation by instead applying the algorithm on a copy of the blurred image rotated 45 degrees counterclockwise and then splicing the resultant image with the recovered image. The resulting spliced image has significantly fewer pixels to interpolate while maintaining the original structure of the image. Results of splicing can be seen in Figure 7.

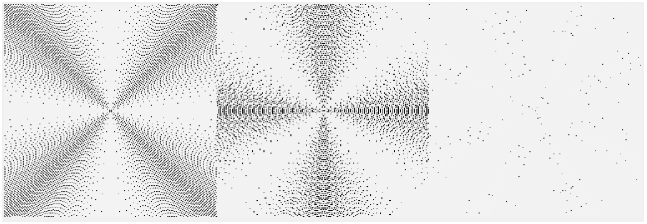

Figure 7: Results of splicing two images together to minimize interpolation

Figure 8 shows a comparison between two different interpolation methods, specific pixel deconvolution and preliminary results from splicing. The specific pixel deconvolution showed a Structural Similarity Index (SSIM) of 0.41 while the results from splicing were 0.476, a significant improvement. Looking at Figure 8, a zoomed in section shows a structure that looks similar to the letter K from the original image and the two results, showing a slight change in shape between the two results and a slight increase in accuracy in the spliced image.

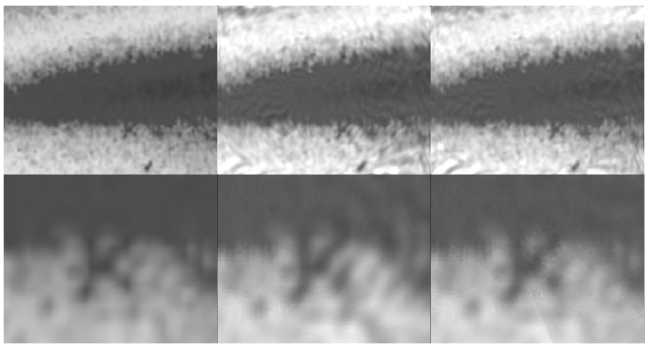

Figure 8: From left to right: original image, specific pixel deconvolution (SSIM 0.41), spliced image (SSIM 0.476)

6 CONCLUSION

Through simulation, the effects of rotational blurring on redline atomic-oxygen-airglow images was investigated and an algorithm was developed to deconvolve the blurring experienced by VIOLET. Several methods of interpolation and specific boundary conditions were investigated as well. The effectiveness of the algorithm combined with effective boundary conditions and interpolation was shown to have a noticeable increase in the quality of the image and further refinement will be done in the future.

Future work will also attempt to incorporate translational blurring into the simulations to include imaging instances where the CubeSat is not imaging parallel to its velocity vector. The computational complexity of the algorithm will be investigated in the future as well as a broader investigation of comparison metrics for images.

ACKNOWLEDGMENTS

Special thanks to CubeSat NB for supporting the research.
The researchers would also like to acknowledge the primary funding provided by the Canadian Space Agency (CSA) and the New Brunswick Innovation Foundation (NBIF)

REFERENCES

[1] Bettina Altmann et al. 2018. Determining Angular Velocities of Fast Rotating Objects Based on Motion Blur to Control an Optomechanical Derotator. *Proceedings in Applied Mathematics and Mechanics* 18, 1 (December 2018). https://doi.org/10.1002/pamm.201800092

[2] Shengyang Dai et al. 2008. Motion from Blur. In *26th IEEE Conference on Computer Vision and Pattern Recognition, CVPR.* Anchorage, AK, USA, 1-8. https://doi.org/10.1109/CVPR.2008.4587582

[3] Rob Garner and Brian Dunbar. 2020. *Hubble Space Telescope Observatory - Pointing Control.* Retrieved October 19, 2021 from https://www.nasa.gov/content/goddard/hubble-space-telescope-pointing-control-system

[4] Rafael C. Gonzalez et al. 2008. *Digital Image Processing Third Edition.* Prentice Hall, Upper Saddle River, N.J.

[5] Per Christian Hansen et al. 2014. Rotational Image Deblurring With Sparse Matrices. *BIT Numerical Mathematics* 54, 3 (September 2014), 649-671. https://doi.org/10.1007/s10543-013-0464-y

[6] Yudan Qiu et al. 2020. End-To-End Rotational Motion Deblurring Method Combining with Motion Information. In *Journal of Physics: Conference Series*, Vol. 1518. IOP Publishing, Sanya, China. https://doi.org/10.1088/1742-6596/1518/1/012038

[7] P. K. Rajesh et al. 2009. First Results of the Limb Imaging of 630.0 nm Airglow Using FORMOSAT-2/Imager of Sprites and Upper Atmospheric Lightnings. *Journal of Geophysical Research: Space Physics* 114, A10 (2009). https://doi.org/10.1029/2009JA014087

[8] W. H. Richardson. 1972. Bayesian-Based Iterative Method of Image Restoration. *Journal of the Optical Society of America* 62, 1 (January 1972), 55-59. https://doi.org/10.1364/JOSA.62.000055

[9] N. Scheidegger. 18/08/2006. Swiss Cube Payload System Engineering DRAFT, Issue 1, Rev 0, École Polytechnique Fédérale de Lausanne, Switzerland. http://escgesrv1.epfl.ch/

[10] Q Shan et al. 2007. Rotational Motion Deblurring of a Rigid Object from a Single Image. In *2007 IEEE 11th International Conference on Computer Vision.* Rio de Janeiro, Brazil, 1-8. https://doi.org/10.1109/ICCV.2007.4408922

[11] David Slepian. 1967. Restoration of photographs blurred by image motion. *The Bell System Technical Journal* 46, 10 (December 1967), 2353-2362. https://doi.org/10.1002/j.1538-7305.1967.tb02461.x

[12] Peter Aundal Toft. 1996. *The Radon Transform - Theory and Implementation.* Ph. D. Dissertation. Technical University of Denmark.

[13] T. Wollmann et al. 2020. Motion Blur Suppression by Using an Optical Derotator for Deformation Measurement of Rotating Components. In *Proceedings of SPIE - The International Society for Optical Engineering*, Vol. 11380. https://doi.org/10.1117/12.2556153

[14] N. Yokota et al. 2010. Blur Estimation For Linear Motion Blurred Image. In *Proceedings of the ISCIE International Symposium on Stochastic Systems Theory and its Applications.* Okayama, Japan, 271-276. https://doi.org/10.5687/sss.2011.271